Network: Comput. Neural Syst. **11** (2000) 221–246. Printed in the UK PII: S0954-898X(00)15111-5

Effects of delay on the type and velocity of travelling pulses in neuronal networks with spatially decaying connectivity

David Golomb†§ and G Bard Ermentrout‡

† Zlotowski Centre for Neuroscience and Department of Physiology, Faculty of Health Sciences, Ben-Gurion University of the Negev, Beer-Sheva 84105, Israel
‡ Department of Mathematics, University of Pittsburgh, Pittsburgh, PA 15260, USA

E-mail: golomb@bgumail.bgu.ac.il

Received 28 March 2000

Abstract. We study a one-dimensional model of integrate-and-fire neurons that are allowed to fire only one spike, and are coupled by excitatory synapses with delay. At small delay values, this model describes a disinhibited cortical slice. At large delay values, the model is a reduction of a model of thalamic networks composed of excitatory and inhibitory neurons, in which the excitatory neurons show the post-inhibitory rebound mechanism. The velocity and stability of propagating continuous pulses are calculated analytically. Two pulses with different velocities exist if the synaptic coupling is larger than a minimal value; the pulse with the lower velocity is always unstable. Above a certain critical value of the constant delay, continuous pulses lose stability via a Hopf bifurcation, and lurching pulses emerge. The parameter regime for which lurching occurs is strongly affected by the synaptic footprint (connectivity) shape. A bistable regime, in which both continuous and lurching pulses can propagate, may occur with square or Gaussian footprint shapes but not with an exponential footprint shape. A perturbation calculation is used in order to calculate the spatial lurching period and the velocity of lurching pulses at large delay values. For strong synaptic coupling, the velocity of the lurching pulse is governed by the tail of the synaptic footprint shape. Moreover, the velocities of continuous and lurching pulses have the same functional dependencies on the strength of the synaptic coupling strength g_{syn}: they increase logarithmically with g_{syn} for an exponential footprint shape, they scale like $(\ln g_{syn})^{1/2}$ for a Gaussian footprint shape, and they are bounded for a square footprint shape or any shape with a finite support. We find analytically how the axonal propagation velocity reduces the velocity of continuous pulses; it does not affect the critical delay. We conclude that the differences in velocity and shape between the front of thalamic spindle waves *in vitro* and cortical paroxysmal discharges stem from their different effective delays.

1. Introduction

Spindle-like discharges propagate in thalamic slices composed of excitatory thalamocortical cells and inhibitory reticular thalamic cells, coupled with reciprocal synaptic connections, in which the excitatory cells possess post-inhibitory rebound mechanisms (see, e.g., Steriade *et al* 1993, von Krosigk *et al* 1993). The propagation velocity is around 1 mm s^{-1} (Kim *et al* 1995). Numerical simulations have indicated that these discharges propagate as *lurching* travelling waves (Destexhe *et al* 1996, Golomb *et al* 1996). At each recruitment cycle, a new group of inhibitory cells is excited, and this group inhibits a new group of excitatory cells. After these cells rebound from hyperpolarization, they excite a new group of cells and a new recruitment

§ Author to whom any correspondence should be addressed. Address for correspondence: Department of Physiology, Faculty of Health Sciences, POB 653, Ben-Gurion University of the Negev, Beer-Sheva 84105, Israel.

0954-898X/00/030221+26$30.00 © 2000 IOP Publishing Ltd

cycle starts. Therefore, the lurching wave has a periodic nature at the front. Rinzel *et al* (1998) have reduced the model of a thalamic slice to a model of coupled inhibitory units, and found that the model can also exhibit a lurching wave if the synaptic reversal potential is high enough. With off-centre inhibition, the lurching wave can propagate in one direction while the continuous wave can propagate in the other direction.

A different type of neuronal population discharge appears in disinhibited coronal neocortical slices in response to electrical stimulation above a certain threshold. These slice preparations were developed initially as experimental models for epilepsy (Connors 1984, Gutnick *et al* 1982). Recently, experimental and theoretical investigations (Ermentrout 1998, Golomb and Amitai 1997, Golomb 1998, Tsau *et al* 1998, Wu *et al* 1999) have tried to relate the dynamics of propagating discharge to the underlying neuronal circuitry, and to use the dynamics of cortical slices as a first stage towards understanding spatio-temporal dynamics in neuronal networks (Nicolelis *et al* 1995, Prechtl *et al* 1997). The average discharge velocity is about 10–15 cm s^{-1} (Golomb and Amitai 1997); neurons are recruited to the wave because of the excitatory recurrent interactions between neurons. Numerical simulations of a conductance-based neuronal model with homogeneous architecture reveal that the discharge propagates at a constant velocity, as a *continuous* travelling pulse (Ermentrout 1998, Golomb and Amitai 1997). Inhomogeneities in the velocity, which were discovered experimentally, were attributed to spatial fluctuations in the synaptic and intrinsic neuronal properties along the slice (Chervin *et al* 1988, Wadman and Gutnick 1993). In both theory and experiment, there was a minimal velocity below which the discharge could not propagate. Propagating discharges with similar properties and velocities have been found in other cortical structures, such as the hippocampus (Miles *et al* 1988, Traub *et al* 1993) and the piriform cortex (Demir *et al* 1998).

In this work, we explore the propagation of the front of these two propagating discharges. Specifically, we ask:

(1) What is the basis for the different types (continuous or lurching) of propagating discharge? How is this type determined by the network architecture, the kinetics of the single cells and synapses, and the synaptic delay?
(2) What is the relationship between the velocity of the pulse (or wave) and the intrinsic, synaptic, and architecture properties of the system?
(3) Does the pulse have a finite minimal velocity with respect to the synaptic coupling?
(4) What are the effects of finite axonal delay on the velocity and the type of propagation?
(5) Why do thalamic networks exhibit slow, lurching discharges whereas cortical networks exhibit fast, continuous discharges?

We develop a joint conceptual framework for the two types of network that enables us to compare the two preparations and the two types of discharge propagation. We show that under certain conditions and approximations, the discharge dynamics of both cortical and thalamic slices can be reduced to a model of integrate-and-fire neurons in which each neuron can fire only one spike. Neurons are coupled by excitatory synapses with delay, which is small for cortical networks and large for thalamic networks. Using analytical and numerical methods, we find that continuous pulses exist and are stable for small values of constant (space-independent) delay. As the constant delay increases, this pulse loses stability and lurching pulses are obtained. Such lurching pulses have not been obtained in models of wave propagation in excitable media with diffusive coupling.

Aspects of the work presented here have appeared in an abstract form (Golomb and Ermentrout 1999a) and in a brief report (Golomb and Ermentrout 1999b). Here we expand on the range of issues covered in the brief report and expound in detail all aspects of our work. Particular emphasis is placed on describing the calculations of the existence, velocity, and

stability of the pulses for several footprint shapes. We have previously found cases for which both continuous and lurching pulses can propagate for the same set of parameters (Golomb and Ermentrout 1999b). Here we test whether this bistability occurs only if the synaptic footprint shape has a finite support. We develop a method for calculating the spatial period of lurching pulses for large delays for every footprint shape. Our results for the integrate-and-fire model with one spike and large delay are compared with simulation results obtained using a conductance-based model of thalamic networks (Golomb *et al* 1996).

2. The model

In this section we first show that for studying fronts of propagating discharges, models of both disinhibited cortical networks and thalamic networks (with excitatory neurons being in the bursting mode) can be reduced to simplified models of chains of integrate-and-fire neurons with delay, in which each neuron can fire only one spike. Then, we describe this model and the numerical methods. Finally, we briefly introduce the conductance-based model of thalamic networks of Golomb *et al* (1996).

2.1. Reduction of models

2.1.1. Reduction of models of paroxysmal discharges in disinhibited cortical networks. Simulations of conductance-based models of paroxysmal discharges in disinhibited cortical slices reveal that the discharge velocity ν is determined primarily by the response of the post-synaptic neuron to the first one or two spikes of the pre-synaptic neuron (Golomb and Amitai 1997), especially with prominent synaptic depression. For example, if we assume that only the first spike elicits an excitatory post-synaptic conductance (EPSC) for the parameters of figure 8 in the work of Golomb and Amitai (1997), the velocity decreases by only 15%. Therefore, with strong depression, taking only the first spike of each pre-synaptic neuron into account and ignoring all the others is a good approximation (Ermentrout 1998). This approximation becomes exact in the case of infinitely strong synaptic depression. Even without strong depression, taking only one spike can be viewed as a simplified way for considering the effects of all the burst discharges of fast spikes together, provided that the synaptic interaction takes into account the combined contribution of all of the spikes of the discharge (a similar approach is used in Wang and Rinzel (1992) and Golomb *et al* (1994, 1996)).

Adjacent cortical neurons have a delay of about 2 ms (Thomson *et al* 1993, Markram *et al* 1997); more distant neurons are expected to have a larger delay because of the finite axonal connectivity. The delay τ_{delay} between neurons at positions x and x' is therefore

$$\tau_{\text{delay}} = \tau_d + \frac{x - x'}{c} \tag{1}$$

where τ_d is the constant delay and c is the axonal conductance velocity. Thus, we include both fixed and distance-dependent delays in the simplified models.

2.1.2. Reduction of models of spindle-like discharges in thalamic networks. We consider a spatially structured network of excitatory neurons, which may be interpreted as a reduction from a two-population thalamic network composed of excitatory thalamocortical (TC) neurons and inhibitory neurons in the thalamic reticular nucleus (RE). The idea is that because the RE-to-TC projection is topographic and acts via $GABA_A$ and $GABA_B$ receptors, excitation of one RE cell would result in a delayed barrage of EPSCs in the neighbouring RE cells through the disynaptic RE–TC–RE loop. In this idealized view of the isolated thalamic circuit, the

RE cell layer acts effectively as a cell population with reciprocal AMPA-mediated excitatory interactions, with an effective delay of order 100 ms caused by the time needed for the TC cell to rebound from inhibition. With the additional axonal delay, the delay in thalamic networks can also be represented by equation (1). Because we are interested in this work only in the recruitment process, we can model the system by considering only the first 'spike' that each cell fires. The large effective delay ensures that the velocity at moderate coupling strengths is determined mainly by the first spike, which represents a Ca^{2+} spike above which rides a train of action potentials (Golomb *et al* 1996). This assumption of fixed effective delay only applies if those TC cells that receive inhibitory input are in burst-capable mode.

2.2. Description of the integrate-and-fire model

We use the following version of the integrate-and-fire (Lapique) model (Tuckwell 1988, Ermentrout 1998, Bressloff 1999, 2000):

$$\frac{\partial V(x,t)}{\partial t} = -\frac{V(x,t)}{\tau_0} + I_{\rm syn}(x,t) + I_{\rm app}(x,t) \tag{2}$$

for $0 < V(x,t) < V_T$, where $V(x,t)$ is the membrane potential of a neuron at a position x and time t, τ_0 is the passive membrane time constant of the neuron, $I_{\rm syn}$ is the normalized synaptic input, and $I_{\rm app}$ is the normalized applied current; $I_{\rm app} = 0$ unless otherwise stated. When V for a neuron reaches the threshold V_T at time $T(x)$, the neuron fires a spike, and cannot fire more spikes afterwards. We assume that the number of neurons within a footprint length is large, and therefore use a continuum model and replace the sum over the pre-synaptic neurons by an integral:

$$I_{\rm syn}(x,t) = g_{\rm syn} \int_{-\infty}^{\infty} {\rm d}x'\; w(x-x')\alpha\left[t - T(x') - \tau_{\rm delay}\right] \tag{3}$$

where $g_{\rm syn} = \tilde{g}_{\rm syn}\Delta/C$, $\tilde{g}_{\rm syn}$ is the synaptic conductance, C is the membrane capacitance, and $\Delta = V - V_{\rm syn}$ is approximated here to be a constant ('coupling by currents'; see, e.g., Ermentrout 1998, Hansel *et al* 1995); $\tau_{\rm delay}$ is the delay between the post- and pre-synaptic neurons. Equations (2), (3) are implicit equations of $T(x)$. The temporal shape of the EPSC that a post-synaptic cell at a position x receives following a spike of a pre-synaptic cell at a position x' is given by the normalized α-function $\alpha[t - T(x')]$:

$$\alpha(t) = \begin{cases} \dfrac{{\rm e}^{-t/\tau_1} - {\rm e}^{-t/\tau_2}}{\tau_1 - \tau_2} & t \geqslant 0 \\ 0 & \text{otherwise} \end{cases} \tag{4}$$

where τ_1 and τ_2 are the synaptic rise and decay time respectively; $\tau_1 \ll \tau_2$. The spatial dependence of the synaptic strength on the distance between neurons, $w(x)$, is denoted as the 'synaptic footprint shape' (Golomb *et al* 1996, Golomb and Amitai 1997). We examine three shapes:

$$w(x) = \frac{1}{2\sigma}{\rm e}^{-|x|/\sigma} \qquad \text{exponential} \tag{5}$$

$$w(x) = \frac{1}{\sqrt{2\pi}\sigma}{\rm e}^{-x^2/(2\sigma^2)} \qquad \text{Gaussian} \tag{6}$$

$$w(x) = \begin{cases} \dfrac{1}{2\sigma} & |x| \leqslant \sigma \\ 0 & |x| > \sigma \end{cases} \qquad \text{square.} \tag{7}$$

σ is called the 'synaptic footprint length'. We consider a half-infinite network; i.e. the length of the system is much larger than σ.

We define the response (Green) function $G(t)$ for $t > 0$ as

$$\frac{\mathrm{d}G}{\mathrm{d}t} = -\frac{G}{\tau_0} + \alpha(t) \qquad G(0) = 0 \tag{8}$$

and $G(t) = 0$ for $t < 0$. Then, for $\tau_1 = 0$,

$$G(t) = \begin{cases} \dfrac{\tau_0}{\tau_0 - \tau_2}(\mathrm{e}^{-t/\tau_0} - \mathrm{e}^{-t/\tau_2}) & t \geqslant 0 \\ 0 & \text{otherwise.} \end{cases} \tag{9}$$

The function G is the normalized excitatory post-synaptic potential (EPSP) developed in the cell as a response to the EPSC (equation (4)). The Volterra representation of equations (2), (3) for neurons that can fire only one spike is

$$\frac{V_T}{g_{\mathrm{syn}}} = \int_{-\infty}^{\infty} \mathrm{d}x'\, w(x') G\left[T(x) - T(x - x') - \tau_d - \frac{x'}{c}\right] \tag{10}$$

together with the condition that $T(x)$ is the first time that the voltage crosses the threshold. This condition requires that V increases with time just before the spike; i.e.,

$$\frac{\mathrm{d}V[x, T(x)]}{\mathrm{d}t} > 0. \tag{11}$$

The meaning of equations (10), (11) is that the summation of all of the contributions to the voltage of one neuron from the other neurons is equal to V_T when this neuron fires, and that this neuron does not fire before.

2.2.1. Numerical methods. Equations (2), (3) are simulated numerically by discretizing space. There are N neurons in the chain, and the density of neurons is ρ in a length σ. The coupled system of ordinary differential equations for the integrate-and-fire neurons is solved using exact integration (Hansel *et al* 1998). To stimulate the network, applied current is 'injected' into a group of neurons on the 'left' of the system (small x-values), that span a length at least equal to the footprint length σ ('shock' initial conditions). A neuron that has fired does not participate any more in the simulation.

2.3. Brief description of the conductance-based thalamic model

Several results of the simplified integrate-and-fire model with a square footprint shape are compared with simulation results of the full RE–TC network model (Golomb *et al* 1996). In this model, each RE cell is represented by a conductance-based scheme including a T-type calcium current, an after-hyperpolarization potassium current, and a leak current. Each TC cell possesses a T-type calcium current, a sag ('h') current, and a leak current. RE cells inhibit TC cells with $\mathrm{GABA_B}$-mediated inhibition (without $\mathrm{GABA_A}$-mediated inhibition), and TC cells excite RE cells with AMPA-mediated excitation. No intra-RE connections are considered. To simulate the conditions on which the integrate-and-fire model is based, each RE cell sends synaptic input to only one TC cell, whereas each TC cell (far from the edges) projects to 17 TC cells; $N = 256$. Open boundary conditions are assumed. The strength of the $\mathrm{GABA_B}$ synapses is $g_{\mathrm{GABA_B}} = 0.06$ mS cm^{-2}. All of the parameters of the model are equal to those given in Golomb *et al* (1996), except for those parameters that are explicitly mentioned.

3. Results

3.1. Continuous and lurching pulses

A pulse can propagate along the network in response to 'shock' initial conditions. For zero or small τ_d (below a critical value τ_{dc}), the pulse is continuous far from the stimulus region (figure 1(A)), and the firing times of the neurons obey $T(x) = T_0 + x/v$, where v is the pulse velocity and T_0 is an arbitrary time. The neuronal potential fulfils an equation for a travelling pulse as well: $V(x,t) = \tilde{V}(x - vt)$ (Golomb and Amitai 1997, Ermentrout 1998). As τ_d approaches a critical value τ_{dc} from below, the convergence of the firing time $T(x)$ to a continuous propagating pulse decelerates. For $\tau_d > \tau_{dc}$, a lurching propagating pulse is observed (figure 1(B)). Space is spontaneously divided into basic spatial units, each with a spatial period length L, and the firing time in each unit can be obtained from the spatial period in the previous unit according to

$$T(x + L) = T(x) + T_{\text{per}} \tag{12}$$

where T_{per} is the time period of a lurching cycle. The average velocity of the pulse is $v = L/T_{\text{per}}$. Suppose that one lurching period starts at $x = 0$ and $T(0) = 0$. The firing time of a neuron at a position x is given by

$$T(x) = nT_{\text{per}} + f(\hat{x}) \tag{13}$$

where n is the integer part of $T(x)/T_{\text{per}}$ (or x/L) and $\hat{x} = x - nL$. The function f, expressing the firing time within one period relative to the starting point of the period in space and time, is defined on the interval $[0, L)$; $f(0) = 0$. Hence, the function

$$T(x) - x/v = f(\hat{x}) - \hat{x}/v \tag{14}$$

is a periodic function of x with a period L. Equation (14) demonstrates the spatio-temporal periodicity of the lurching pulse.

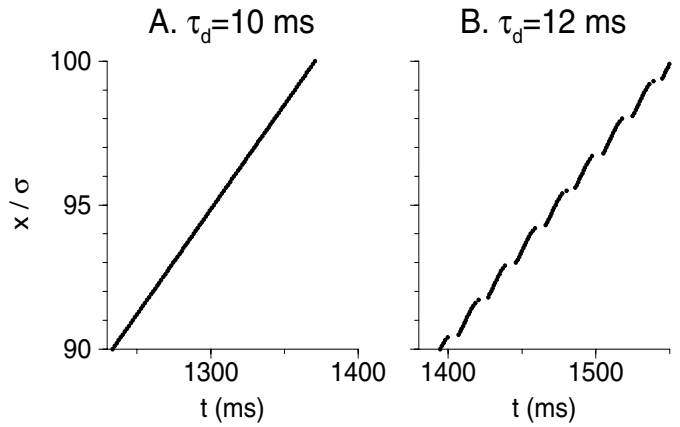

Figure 1. Rastergrams obtained from simulating equations (2), (3), (5), with the condition that each neuron can fire only one spike. The solid circles represent the firing time of neurons as a function of their normalized position x/σ; spikes of only one out of every five neurons are plotted. Together, the groups of solid circles looks almost like one continuous line. Parameters: $\tau_0 = 30$ ms, $\tau_2 = 2$ ms, $g_{\text{syn}}/V_T = 10$, $c/\sigma = 5$ ms^{-1}, $N = 5000$, $\rho = 50$. For these parameters, $\tau_{dc} = 11.15$ ms. (A) For $\tau_d < \tau_{dc}$ (10 ms), a continuous pulse is obtained. (B) For $\tau_d > \tau_{dc}$ (12 ms), the pulse is lurching.

In the following, we calculate first the existence and stability regimes and the velocity of the continuous and lurching pulses for $c \to \infty$. In most calculations we will take $\tau_1 = 0$ for simplicity. The effects of finite τ_1 will be specifically evaluated. Then, we analyse the effects of finite axonal velocity c. Finally, we show that several effects discovered in the integrate-and-fire model are demonstrated also in conductance-based models of thalamic networks.

3.2. Existence, stability and velocity of continuous pulses

3.2.1. General formalism. Substituting the condition for a continuous pulse, $T(x) = x/\nu$, into the evolution equation (10), we obtain

$$\int_0^\infty \mathrm{d}x'\; w(x' + \tau_d \nu) G(x'/\nu) = V_T / g_{\mathrm{syn}}. \tag{15}$$

We should also confirm that the condition of equation (11) holds. Stability of the continuous pulse is calculated by considering $T(x) = x/\nu + s(x)$ and linearizing equation (10) near the continuous solution, to obtain

$$\int_0^\infty \mathrm{d}x'\; w(x' + \tau_d \nu) G'(x'/\nu) \left[s(x) - s(x - x' - \tau_d \nu) \right] = 0. \tag{16}$$

This convolution equation has a general solution $s(x) = \exp(\lambda x)$. Substituting this equation in equation (16) yields

$$\int_0^\infty \mathrm{d}x'\; w(x' + \tau_d \nu) G'(x'/\nu) \left[1 - \mathrm{e}^{-\lambda(x' + \tau_d \nu)} \right] = 0. \tag{17}$$

$\lambda = 0$ is always a solution to equation (17), because of the translation invariance of the continuous pulse. The continuous wave is stable if $\mathrm{Re}\,\lambda < 0$ for all the λ-values that are solutions of this eigenvalue equation (except for that single zero solution). This means that a small perturbation at a specific, finite x will decay at larger x as the pulse propagates. A similar method for studying stability was developed independently by Bressloff (1999, 2000).

3.2.2. Exponential footprint shape. The velocity ν is determined using equations (5), (9), (15):

$$\frac{(\tau_0 \nu + \sigma)(\tau_2 \nu + \sigma)}{\tau_0 \nu \sigma} \exp\left(\frac{\tau_d \nu}{\sigma} \right) = \frac{g_{\mathrm{syn}}}{2 V_T}. \tag{18}$$

This is an extension of the equation obtained in Ermentrout (1998) for $\tau_d = 0$. From this equation, one can see that:

(1) For $\tau_d = 0$, the left-hand side of equation (18) has a minimum with respect to ν at $\nu_{\min} = \sigma / \sqrt{\tau_0 \tau_2}$. Continuous pulses cannot propagate below this minimal velocity, which is obtained for a minimal synaptic coupling $g_{\mathrm{syn,min}}$. For $g_{\mathrm{syn}} > g_{\mathrm{syn,min}}$, there are two branches of solutions to equation (18). In the fast branch, ν increases with g_{syn}, and in the slow branch ν decreases with g_{syn} (Ermentrout 1998).
(2) Because $\exp(\tau_d \nu / \sigma) > 1$ and increases with τ_d, $\nu_{\min}$ decreases with τ_d and is obtained for larger $g_{\mathrm{syn,min}}$.
(3) For $\tau_d > 0$ and at large enough g_{syn}, the velocity is determined mainly by the exponential factor in equation (18), and therefore ν depends logarithmically on g_{syn} to the highest order. In contrast, for $\tau_d = 0$, the velocity exhibits a power-law dependence on g_{syn} at large g_{syn} (Ermentrout 1998). Graphs of ν/σ as a function of V_T / g_{syn} for $\tau_d = 0$ and $\tau_d = 10$ ms are shown in figure 2(A).

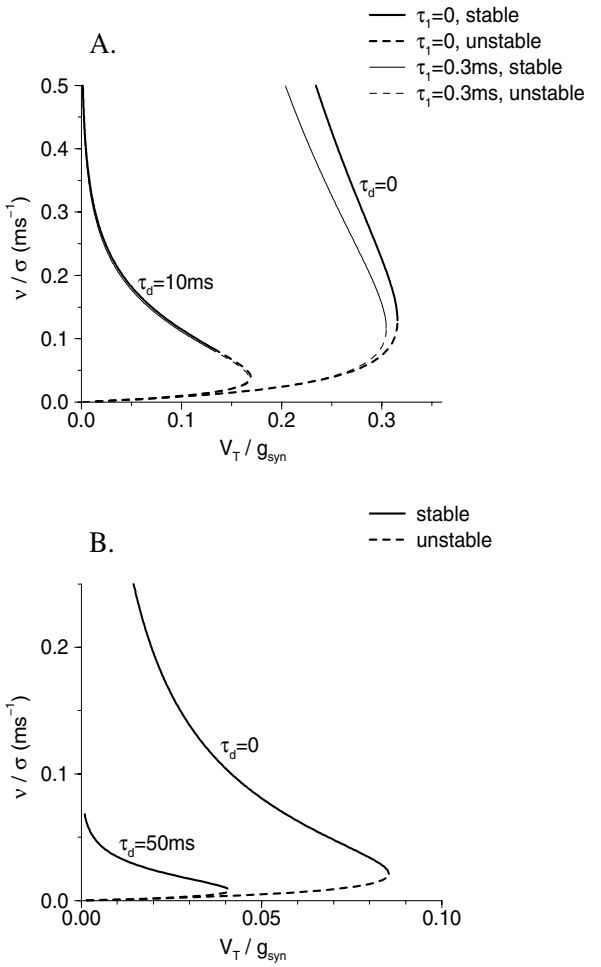

Figure 2. Exponential footprint shape. The velocity of the continuous pulse is plotted as a function of $V_T/g_{\rm syn}$. Solid lines represent stable pulses and the dashed lines represent unstable pulses. (A) Parameters: $\tau_0 = 30$ ms, $\tau_2 = 2$ ms. Wide lines denote graphs with $\tau_1 = 0$, and narrow lines denote graphs with $\tau_1 = 0.3$ ms. Calculations are done for two values of τ_d: 0 (right curves) and 10 ms (left curves). For $\tau_1 = 10$ ms, the graphs for $\tau_1 = 0$ and $\tau_1 = 0.3$ ms almost overlap. The velocity is calculated according to equations (18), (25), and the stability is determined from equations (23), (24), (26). (B) Parameters: $\tau_0 = 30$ ms, $\tau_1 = 5$ ms, $\tau_2 = 50$ ms; these parameters correspond to NMDA synaptic kinetics. Calculations are done for two values of τ_d: 0 (right curve) and 50 ms (left curve). For $\tau_d = 50$ ms, the lower part of the upper branch is unstable; this is hardly visible in the graph.

In order to find the function $V(x, t)$ before the spike (and thus verify that (11) holds), we look without loss of generality at a neuron located at $x = 0$. The Volterra representation of equations (2), (3) for the travelling wave $T(x) = x/\nu$ for time $t < 0$, taking into account that $G(t) = 0$ for $t < 0$, is

$$V(0,t) = g_{\rm syn}\int_{-\infty}^{\infty} {\rm d}x'\, w(x')G\left[t - T(-x') - \tau_d\right] = g_{\rm syn}\int_{(\tau_d - t)\nu}^{\infty} {\rm d}x'\, w(x')G\left(t + \frac{x}{\nu} - \tau_d\right). \tag{19}$$

Substituting equations (5), (9) into equation (19) yields

$$V(0,t) = \frac{g_{\rm syn}\tau_0\nu\sigma}{2(\tau_0\nu+\sigma)(\tau_2\nu+\sigma)}\exp\left[\frac{(t-\tau_d)\nu}{\sigma}\right]. \tag{20}$$

The voltage V rises exponentially from 0 and reaches V_T at $t = 0$ for all ν-values; both the upper and lower branches fulfil† the condition of equation (11).

The stability of the continuous pulse is explored by substituting equations (5), (9) in equation (17) to obtain

$$e^{\lambda\nu\tau_d} = \frac{(\tau_0\nu+\sigma)(\tau_2\nu+\sigma)(1+\lambda\sigma)}{[\tau_0\nu(1+\lambda\sigma)+\sigma][\tau_2\nu(1+\lambda\sigma)+\sigma]}. \tag{21}$$

As mentioned above, $\lambda = 0$ is always a root due to translation invariance. In appendix A we show in general that the lower branch, for which $d\nu/dg_{\rm syn} < 0$, is unstable. This can be easily demonstrated in the case $\tau_d = 0$, in which there is another solution to equation (21), $\lambda = \sigma/(\nu^2\tau_0\tau_2) - 1/\sigma$. The pulse is stable if $\nu > \sigma/\sqrt{\tau_0\tau_2}$, and therefore the fast branch is stable and the slow branch is unstable.

In order to examine whether the delay can destabilize pulses that belong to the fast branch, we look for a pair of complex conjugate eigenvalues which cross the imaginary axis. If this occurs, we generically expect a Hopf bifurcation to periodic solutions (lurching waves) for the functional equation (15). At this point $\lambda = i\omega$, and

$$e^{i\omega\nu\tau_{dc}} = \frac{(\tau_0\nu+\sigma)(\tau_2\nu+\sigma)(1+i\omega\sigma)}{[\tau_0\nu(1+i\omega\sigma)+\sigma][\tau_2\nu(1+i\omega\sigma)+\sigma]} \equiv Z(\omega). \tag{22}$$

As ω varies, the left-hand side traces out the unit circle. In order to solve this equation, we search for the non-zero ω-value for which $|Z(\omega)| = 1$. This value is given by

$$\omega^2 = \left[\sigma^4 + 2\sigma^3\nu(\tau_0+\tau_2) + 4\sigma^2\nu^2\tau_0\tau_2 - \nu^4\tau_0^2\tau_2^2\right]/(\sigma^2\nu^4\tau_0^2\tau_2^2). \tag{23}$$

For that ω we find τ_{dc}, the critical value of τ_d for which the arguments of the complex numbers on the two sides of equation (22) are equal:

$$\tau_{dc} = \frac{\arg[Z(\omega)]}{\omega\nu}. \tag{24}$$

Note that τ_{dc} does not depend explicitly on $g_{\rm syn}$, but only through ν. Using equations (23), (24), τ_{dc} is calculated as a function of ν. This solution shows that τ_{dc} increases with ν, and this increase is steep at small ν and modest at large ν. As a result, for small values of τ_d, the Hopf bifurcation occurs on the lower, slow branch and does not have an effect on the dynamics. For larger values of τ_d, the Hopf bifurcation occurs on the upper, fast branch, and the continuous pulse is unstable for low velocities, as shown in figure 2(A).

3.2.3. Behaviour near the bifurcation. In order to study the transition from a continuous pulse to a lurching pulse near the critical delay τ_{dc}, we calculated analytically the velocity of the pulse (equation (18)) and compared it with the velocity computed using numerical simulations, as shown in figure 3(A). For $\tau_d \geqslant \tau_{dc}$, the velocity of the lurching pulse is slightly higher than the velocity of the unstable continuous pulse. The difference between the velocity of the pulse obtained in simulations and the velocity of the continuous pulse is shown in figure 3(B). For $\tau_d \leqslant \tau_{dc}$, it is 0. For $\tau_d \geqslant \tau_{dc}$, the differences in velocities increase linearly with $\tau_d - \tau_{dc}$. The continuous dependence of this velocity difference on $\tau_d - \tau_{dc}$ suggests that the Hopf bifurcation is supercritical. The calculation of the normal form of the bifurcation is very tedious, and is not carried out here.

† In Golomb and Ermentrout (1999b), we erroneously claimed that the lower branch is not meaningful.

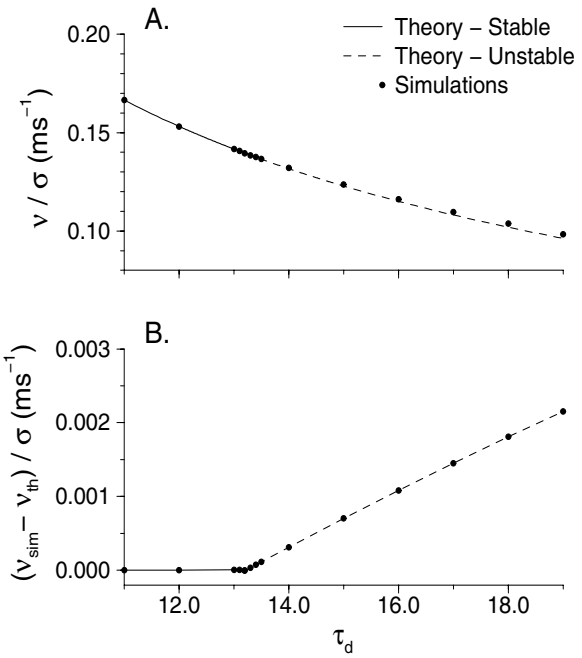

Figure 3. Pulse velocities of the continuous and lurching pulses are plotted as a function of τ_d near the critical delay τ_{dc}. Parameters: $\tau_0 = 30$ ms, $\tau_2 = 2$ ms, $g_{\rm syn}/V_T = 20$, $c \to \infty$; for these parameters, $\tau_{dc} = 13.23$ ms. (A) The velocity of the continuous pulse (solid line: stable; dashed line: unstable) calculated from equation (18), and the velocity of the wave that is actually obtained in simulations with $N = 10^5$ and $\rho = 500$ (solid dots). For $\tau_d > \tau_{dc}$, the velocity of the lurching pulse deviates from the analytical result for the continuous pulse. (B) The difference between the velocity of the waves in simulations. The differences are 0 for the continuous pulse; they increase linearly with $\tau_d - \tau_{dc}$ for $\tau_d > \tau_{dc}$. The solid dots represent the τ_d-values for which simulations were made. These dots are connected by a solid line in the regime where the continuous pulses are stable, and by a dashed line in the regime where the continuous pulses are unstable. Note that lines in (A) correspond to analytic solutions, while in (B) they just connect the dots.

3.2.4. Finite rise time τ_1. Until now, the synaptic rise time has been assumed to be instantaneous. In order to assess the effects of finite τ_1, we calculate the velocity of the continuous pulse for any τ_1 and obtain

$$\frac{(\tau_0\nu+\sigma)(\tau_1\nu+\sigma)(\tau_2\nu+\sigma)}{\tau_0\nu\sigma^2}\exp\left(\frac{\tau_d\nu}{\sigma}\right)=\frac{g_{\rm syn}}{2V_T}. \tag{25}$$

The critical delay above which the continuous pulse is unstable is given by

$$e^{i\omega\nu\tau_{dc}}=\frac{(\tau_0\nu+\sigma)(\tau_1\nu+\sigma)(\tau_2\nu+\sigma)(1+i\omega\sigma)}{[\tau_0\nu(1+i\omega\sigma)+\sigma]\,[\tau_1\nu(1+i\omega\sigma)+\sigma]\,[\tau_2\nu(1+i\omega\sigma)+\sigma]}. \tag{26}$$

The dependence of ν on $g_{\rm syn}$ and the stability of the continuous pulses are shown in figure 2(A) for $\tau_1 = 0.3$ ms and delay values $\tau_d = 0$ and $\tau_d = 10$ ms. Without delay, the velocity at high $g_{\rm syn}$ is substantially lower for finite τ_1. This is a result of the fact that at high $g_{\rm syn}$, ν scales linearly with $g_{\rm syn}$ for $\tau_1 = 0$ but as $\sqrt{g_{\rm syn}}$ for $\tau_1 > 0$ (Ermentrout 1998). The situation is different, however, for finite values of τ_d; even for $\tau_d = 10$ ms, the graph of ν versus $g_{\rm syn}$ for $\tau_1 = 0.3$ ms almost overlaps the corresponding graph for $\tau_1 = 0$. Indeed, equation (25) shows that in both cases, $\nu \simeq \ln(g_{\rm syn})$ at high $g_{\rm syn}$. We conclude that even for moderate values of τ_d,

small but finite τ_1-values do not have a significant effect on the velocity and stability of the continuous pulse.

Increasing τ_2 to 50 ms and τ_1 to 5 ms, to mimic the NMDA synaptic kinetics (Fleidervish *et al* 1998), reduces the minimal velocity $\nu_{\min}$ (figure 2(B)). In addition, larger τ_d-values are needed for destabilizing the continuous pulses. For example, for $\tau_d = 50$ ms, $g_{\mathrm{syn,c}}$ is only slightly larger than $g_{\mathrm{syn,min}}$ ($25.4V_T$ and $24.3V_T$ respectively).

3.2.5. Square footprint shape. The velocity ν is determined using equations (7), (9), (15):

$$\frac{2V_T}{g_{\mathrm{syn}}} = \frac{\tau_0\nu}{\sigma}\left\{1 - \frac{1}{\tau_0 - \tau_2}\left[\tau_0 \exp\left(\frac{\tau_d - \sigma/\nu}{\tau_0}\right) - \tau_2 \exp\left(\frac{\tau_d - \sigma/\nu}{\tau_2}\right)\right]\right\}. \tag{27}$$

Graphs of ν/σ as a function of V_T/g_{syn} for several values of τ_d are shown in figure 4. The qualitative results regarding the minimal velocity and its dependence on τ_d are the same as for the exponential case. The situation is different, however, for large g_{syn}. For $\nu = \sigma/\tau_d$, the right-hand side of equation (27) is zero. Hence, at the limit $g_{\mathrm{syn}} \to \infty$ the velocity of the continuous pulse approaches the finite value σ/τ_d.

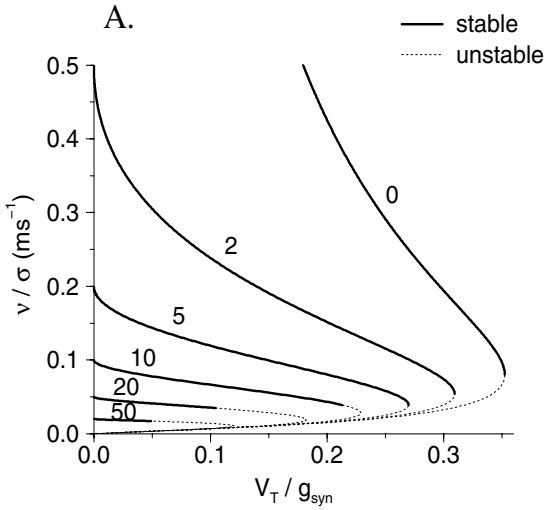

Figure 4. Square footprint shape; parameters: $\tau_0 = 30$ ms, $\tau_2 = 2$ ms. The velocity of the continuous pulse as a function of V_T/g_{syn} for several values of τ_d. The wide solid lines represent stable pulses and the narrow dotted lines represent unstable pulses. The number above each line, from 0 to 50, denotes the value of τ_d. The velocity is calculated according to equation (27), and the stability is determined numerically on the basis of equation (28).

The stability of the continuous pulse is explored by substituting equations (7), (9) in equation (17) to obtain

$$\begin{aligned}(1+\lambda\tau_0\nu)(1+\lambda\tau_2\nu)&\left[\exp\left(\frac{\tau_d - \sigma/\nu}{\tau_0}\right) - \exp\left(\frac{\tau_d - \sigma/\nu}{\tau_2}\right)\right] \\ &= \lambda\nu(\tau_0 - \tau_2)\exp(-\lambda\tau_d\nu) + \left[(1+\lambda\tau_2\nu)\exp\left(\frac{\tau_d - \sigma/\nu}{\tau_0}\right)\right. \\ &\quad \left. - (1+\lambda\tau_0\nu)\exp\left(\frac{\tau_d - \sigma/\nu}{\tau_2}\right)\right]\exp(-\sigma\lambda).\end{aligned} \tag{28}$$

To calculate the τ_{dc}-value for which the continuous pulse becomes unstable, we substitute $\lambda = \mathrm{i}\omega$ in equation (28) and obtain two real transcendental equations for the real variables τ_{dc} and ω. We solve these equations numerically for one large enough value of ν using standard iteration methods (Press *et al* 1992). The fact that ω, which is the spatial period of the expanding or decaying fluctuations, is of order $2\pi/\sigma$ helps us to choose initial conditions for the iteration process. At small ν, it is numerically difficult to use this method to solve the equations. Therefore, we write ordinary differential equations with these two equations as their nullclines, and follow the their fixed-point solution using the program XPPAUT (Doedel 1981, Rinzel and Ermentrout 1998), starting from the solution at large ν that we have already computed. Using equation (27), we calculate the range of stability as a function of g_{syn} and τ_d. Our numerical calculation indicates that the critical delay τ_{dc} increases with g_{syn} linearly at large g_{syn} (not shown). As a result, for a specific τ_d, there is a moderate g_{syn}-value for which the continuous pulse is stable, as shown in figure 4.

Numerical investigation of the regime in the τ_d–g_{syn} plane in which lurching pulses are obtained (Golomb and Ermentrout 1999b) revealed two apparent differences between the situations in the case of square footprint shape and the case of exponential footprint shape. First, lurching pulses exist in an area which is composed of 'tongues'. Second, a *bistable* regime exists, in which the two types of pulse can propagate, depending on the initial stimulation. This bistability suggests that the Hopf bifurcation in which the continuous pulse loses stability is subcritical.

3.2.6. Gaussian footprint shape. One major difference between the square and the exponential footprint shapes is that the first shape has a finite support whereas the second shape does not. Is the existence of bistability and tongues in the square case a result of the finite support? In order to answer this question, we examine a third shape: a Gaussian, which decays in space faster than exponentially but does not have a finite support.

The velocity ν for the Gaussian shape is determined using equations (6), (9), (15):

$$\frac{2V_T}{g_{\mathrm{syn}}} = \frac{\tau_0}{\tau_0 - \tau_2}\left[\exp\left(\frac{\tau_d}{\tau_0} + \frac{\sigma^2}{2\nu^2\tau_0^2}\right)\mathrm{erfc}\left(\frac{\tau_d\nu}{\sqrt{2}\sigma} + \frac{\sigma}{\sqrt{2}\nu\tau_0}\right) - \exp\left(\frac{\tau_d}{\tau_2} + \frac{\sigma^2}{2\nu^2\tau_2^2}\right)\mathrm{erfc}\left(\frac{\tau_d\nu}{\sqrt{2}\sigma} + \frac{\sigma}{\sqrt{2}\nu\tau_2}\right)\right] \tag{29}$$

where

$$\mathrm{erfc}(z) = (2/\sqrt{\pi})\int_z^\infty \exp(-t^2)\,\mathrm{d}t.$$

At large ν and g_{syn}, we use the approximation

$$\mathrm{erfc}(z) \approx \mathrm{e}^{-z^2}/(\sqrt{\pi}z) \tag{30}$$

to obtain

$$\frac{2V_T}{g_{\mathrm{syn}}} \approx \frac{\sqrt{2}\tau_0\sigma^3\nu}{\sqrt{\pi}(\tau_d\tau_0\nu^2 + \sigma^2)(\tau_d\tau_2\nu^2 + \sigma^2)}\exp\left(-\frac{\tau_d^2\nu^2}{2\sigma^2}\right). \tag{31}$$

The velocity ν scales as $\sqrt{\ln(g_{\mathrm{syn}})}$ to the highest order.

The stability of the continuous pulse is explored by substituting equations (6), (9) in

equation (17) to obtain

$$\tau_0 \exp\left(\frac{\tau_d}{\tau_2}+\frac{\sigma^2}{2\nu^2\tau_2^2}\right)\operatorname{erfc}\left(\frac{\tau_d\nu}{\sqrt{2}\sigma}+\frac{\sigma}{\sqrt{2}\nu\tau_2}\right)-\tau_2\exp\left(\frac{\tau_d}{\tau_0}+\frac{\sigma^2}{2\nu^2\tau_0^2}\right)\operatorname{erfc}\left(\frac{\tau_d\nu}{\sqrt{2}\sigma}+\frac{\sigma}{\sqrt{2}\nu\tau_0}\right)$$
$$=\tau_0\exp\left(\frac{\tau_d}{\tau_2}+\frac{\sigma^2}{2\nu^2\tau_2^2}+\frac{\sigma^2\lambda^2}{2}+\frac{\lambda}{\nu\tau_2}\right)\operatorname{erfc}\left(\frac{\tau_d\nu}{\sqrt{2}\sigma}+\frac{\sigma}{\sqrt{2}\nu\tau_2}+\frac{\sigma\lambda}{\sqrt{2}}\right)$$
$$-\tau_2\exp\left(\frac{\tau_d}{\tau_0}+\frac{\sigma^2}{2\nu^2\tau_0^2}+\frac{\sigma^2\lambda^2}{2}+\frac{\lambda}{\nu\tau_0}\right)\operatorname{erfc}\left(\frac{\tau_d\nu}{\sqrt{2}\sigma}+\frac{\sigma}{\sqrt{2}\nu\tau_0}+\frac{\sigma\lambda}{\sqrt{2}}\right). \qquad (32)$$

As in the case of the square footprint shape, we calculate τ_{dc} by substituting $\lambda = \mathrm{i}\omega$ in equation (32). The two transcendental real equations for τ_{dc} and ω are solved using the function `FindMinimum` of the software package Mathematica (Wolfram 1996). The different behavioural regimes of the continuous pulse for a Gaussian footprint shape are presented in figure 5(A). The solid line denotes the values of g_{syn} and τ_d for which the minimal possible

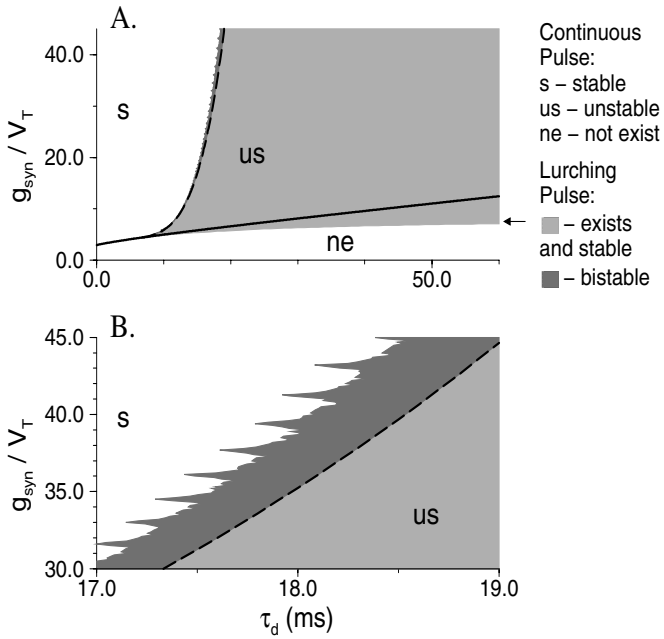

Figure 5. Gaussian footprint shape; parameters: $\tau_0 = 30$ ms, $\tau_2 = 2$ ms. (A) Regimes of existence and stability of the continuous and lurching pulses are shown in the τ_d–g_{syn} plane. The boundaries of the regime in which the lurching pulse exists and is stable were computed from numerical simulations, in which a pulse was initiated by a 'shock' initial stimulus; $N = 20\,000$, $\rho = 50$. The solid line denotes the values of g_{syn} and τ_d for which the minimal possible velocity $g_{\mathrm{syn,min}}$ is obtained; At lower g_{syn}-values, the pulse cannot propagate. The continuous pulse becomes unstable (via a Hopf bifurcation) on the dashed line of critical delay values τ_{dc}. The continuous pulse is therefore stable above both the solid and the dashed line, as denoted by 's'. It is unstable between the two lines, as denoted by 'us', and does not exist below the continuous line, as denoted by 'ne'. The light-grey shading represents the region for which lurching pulses (and not continuous pulses) are obtained. The arrow to the right of the graph represents the minimal values of g_{syn} for which the lurching pulse is found in simulations for $\tau_d \to \infty$. There is a bistable regime, in which the continuous pulse coexists with the lurching pulse. This regime has a 'tongue-like' structure; it is denoted by the dark-grey shading. (B) The bistable regime, that has a 'tongue-like' structure, is narrow; it is shown here on a magnified scale.

velocity $g_{\mathrm{syn,min}}$ is obtained; at lower g_{syn}-values, the pulse cannot propagate. The continuous pulse becomes unstable (via a Hopf bifurcation) on the dashed line of critical delay values τ_{dc}. The continuous pulse is therefore stable above both the solid and the dashed line, as denoted by 's'. It is unstable between the two lines, as denoted by 'us', and does not exist below the continuous line, as denoted by 'ne'. The light-grey shading represents the region for which lurching pulses (and not continuous pulses) are obtained. There is a narrow bistable regime in which both the continuous pulse and the lurching pulse can propagate. This regime, which is denoted by the dark-grey shading, is better displayed in figure 5(B) on a magnified parameter scale. The bistable regime exhibits tongues, but their area in the τ_d–g_{syn} plane is smaller in comparison to the case of the square footprint shape. The existence of a bistable regime and tongues in this case shows that they can appear even when the footprint extends infinitely in both directions.

3.3. Velocity of lurching pulses

How does the velocity of the lurching pulse depend on the synaptic strength? We can calculate this velocity in the case where

$$\tau_2 \ll \tau_0 \ll \tau_d. \tag{33}$$

This case corresponds to a large delay and fast EPSCs (as in thalamic slices); note that $\tau_1 = 0$. Simulations of such cases show that neurons fire only during a time period that is small in comparison to the delay, and L is almost unaffected by the delay period as long as the delay is large enough. Therefore, the pulse velocity is $v = L/\tau_d$. For $\tau_d \gg \tau_0$, a neuron that fires during the nth lurching period (with length L and time T_{per}) is affected only by neurons that have fired during the previous lurching period. The contribution to the potential of that neuron of neuronal EPSCs from neurons in earlier periods has already decayed, mostly because of the large delay and also because of the fact that neurons in earlier lurching periods are more distant from that neuron. The neuron is also not affected by neurons that fire during the same lurching period. We assume that the lurching wave is initiated at very large, negative x, and a lurching spatial period starts at $x = 0$. Neurons at a position $0 \leqslant x < L$ will be affected only by neurons located in the interval $-L \leqslant x < 0$. From the definition of the function $f(x)$ (equation (13)), we see that $T(x) = f(x)$ for $0 \leqslant x < L$ and $T(x) = f(x) - T_{\mathrm{per}}$ for $-L \leqslant x < 0$. Equation (10) for neurons at $0 \leqslant x < L$ becomes

$$\frac{V_T}{g_{\mathrm{syn}}} = \int_{-L}^{0} \mathrm{d}x'\, w(x - x') G\left[f(x) - f(x') + \hat{T} \right] \tag{34}$$

where $\hat{T} = T_{\mathrm{per}} - \tau_d$. In all of the simulations that we have performed, we found that $\hat{T} > 0$. Here we calculate L by considering neurons with $x \leqslant L$ such that the argument of G in equation (34) is non-negative. Substituting equation (9) in (34) we obtain

$$\frac{V_T}{g_{\mathrm{syn}}} = \int_{0}^{L} \mathrm{d}x'\, w(x - x' + L) \frac{\tau_0}{\tau_0 - \tau_2} \left\{ \mathrm{e}^{-[f(x) - f(x') + \hat{T}]/\tau_0} - \mathrm{e}^{-[f(x) - f(x') + \hat{T}]/\tau_2} \right\}. \tag{35}$$

We continue by using the condition $\epsilon \equiv \tau_2/\tau_0 \ll 1$. Using the *ansatz*

$$\hat{T} = \mathrm{O}(\epsilon) \qquad f(x) = \mathrm{O}(\epsilon) \tag{36}$$

we define the scaled function and variable

$$\phi(x) = f(x)/\epsilon \qquad \theta = \hat{T}/\epsilon. \tag{37}$$

This assumption is supported by the simulations for the exponential footprint shape shown in figure 6, where the function $\phi(x)$ is plotted for several values of τ_2 (A), and θ is plotted as a

function of τ_2 (B). In is seen that $\phi(x)$ converges to a constant function as ϵ decreases, and θ converges to a limit value. Because $\exp\{\epsilon[\phi(x) - \phi(x') + \theta]/\tau_0\} \simeq 1$, equation (35) becomes approximately

$$\frac{V_T}{g_{\rm syn}} \simeq \int_0^L {\rm d}x'\ w(x - x' + L) - {\rm e}^{[\theta - \phi(x)]/\tau_0} \int_0^L {\rm d}x'\ w(x - x' + L){\rm e}^{\phi(x')/\tau_0}. \tag{38}$$

As x approaches L, ϕ increases. At the point where the firing time $T(x)$ diverges (or at least becomes larger than τ_d), the lurching spatial period ends. In order to find L, we let $\phi(x) \to \infty$ as $x \to L$, and hence $\lim_{x\to L} \exp[-\phi(x)/\tau_0] = 0$. Therefore, taking at the limit $x \to L$, equation (38) yields, after a change of variables,

$$\frac{V_T}{g_{\rm syn}} = \int_L^{2L} {\rm d}x\ w(x). \tag{39}$$

This is an implicit equation for L under the conditions of equation (33). The RHS of equation (39) is zero for $L = 0$ and for $L \to \infty$ (because $w(x)$ vanishes at large L-values), and is non-negative for finite L. Therefore, it reaches a finite maximum at finite L. If $g_{\rm syn}$ is smaller than its value at that maximum, no lurching pulse can propagate, and therefore the lurching pulse has a threshold. If $g_{\rm syn}$ is above this threshold value, there are (at least) two solutions to equation (39). We consider only the solution for which ${\rm d}L/{\rm d}g_{\rm syn} > 0$. The second solution is probably unstable; this has yet to be proven. Here we discuss several specific footprint shapes.

3.3.1. Exponential footprint shape. By substituting equation (5) in equation (39), one obtains

$$L = \sigma \ln 2 - \sigma \ln(1 - \sqrt{1 - 8V_T/g_{\rm syn}}). \tag{40}$$

For large $g_{\rm syn}$, expanding equation (40) yields

$$L = \sigma \ln\left(\frac{g_{\rm syn}}{2V_T}\right). \tag{41}$$

Equation (40) has a solution only if $g_{\rm syn} > 8V_T$, which is the synaptic conductance threshold. The theoretical result obtained here coincides exactly with simulation results (Golomb and Ermentrout 1999b).

3.3.2. Gaussian footprint shape. By substituting equation (6) in equation (39), one obtains

$$\frac{2V_T}{g_{\rm syn}} = {\rm erfc}\left(\frac{L}{\sqrt{2}\sigma}\right) - {\rm erfc}\left(\frac{\sqrt{2}L}{\sigma}\right). \tag{42}$$

For large $g_{\rm syn}$ and large L, we use the approximation of equation (30) and obtain

$$\frac{L^2}{2\sigma^2} + \ln\frac{L}{\sigma} = \ln\frac{g_{\rm syn}}{V_T} - \frac{1}{2}\ln(2\pi). \tag{43}$$

This means that L scales at very large $g_{\rm syn}$ as $\sqrt{\ln(g_{\rm syn})}$, with some logarithmic corrections.

The dependence of the lurching spatial period L (in units of σ) as a function of $g_{\rm syn}/V_T$ is shown in figure 7. The bent solid line on the logarithmic scale shows that L increases less than logarithmically with $g_{\rm syn}$. The open circles represent simulation results with $\tau_d = 1000$ ms, $\tau_0 = 30$ ms, and $\tau_2 = 0.002$ ms, and they fall exactly on the analytical curve.

Using simulations, we tested the validity of the perturbation calculation when the time constants of the system do not fulfil equation (33). First, we reduced τ_d to 20 ms. This change has almost no effect for large $g_{\rm syn}$, and mildly increases L for small $g_{\rm syn}$. This velocity increase can be attributed to the excitatory effect on a neuron from neurons in cycles before

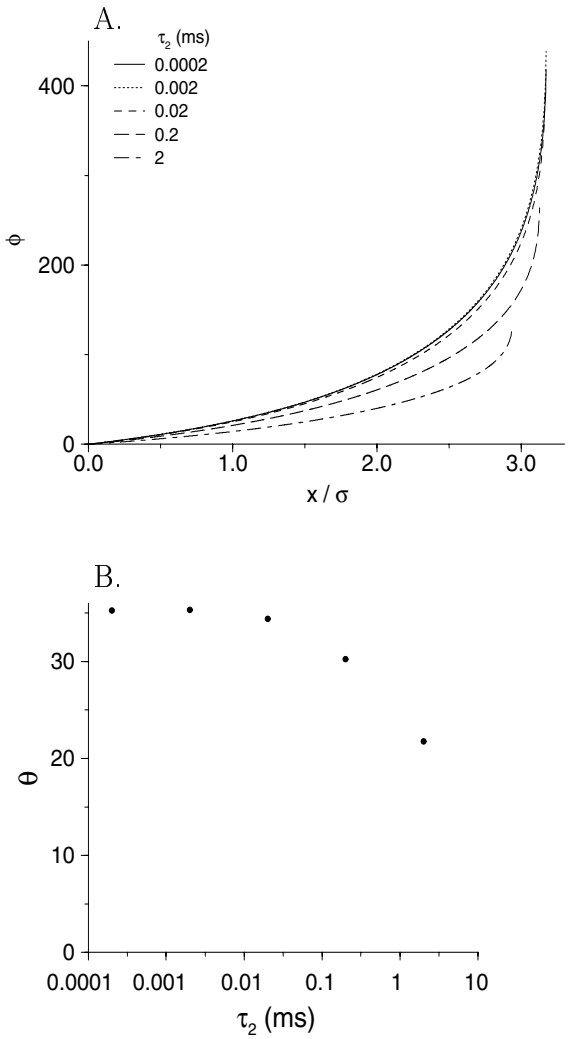

Figure 6. (A) The function $\phi(x)$ versus x/σ for several values of τ_2. The values of τ_2 (in ms) are: 0.0002 (solid line), 0.002 (dotted line), 0.02 (dashed line), 0.2 (long-dashed line) and 2 (dotted–dashed line). The curve for $\tau_2 = 0.0002$ ms is almost identical to the curve for $\tau_2 = 0.002$ ms. (B) θ as a function of τ_2. Results for both (A) and (B) were obtained from simulations with $\tau_d = 1000$ ms, $\tau_0 = 30$ ms, $N = 50\,000$, $\rho = 500$. These simulations show that $\phi(x)$ and θ reach limit values as $\tau_2 \to 0$.

the immediate previous lurching cycle; it is stronger for small g_{syn} because of the shorter L. Second, we increased τ_2 to 2 ms. As a result, L decreases somewhat, because the EPSP developed in the post-synaptic cell (equation (8)) is smaller as a result of the interplay between the EPSC and the leaky neuronal integrator. Third, we simulated a network with $\tau_1 = 0.3$ ms. This finite rise time did not change L significantly in comparison to the case for $\tau_1 = 0$. Note that for $\tau_2 = 2$ ms, continuous (and not lurching) pulses propagate for the third and fourth parameter sets of figure 7 at high g_{syn}-values; we do not show simulation results when lurching pulses are not obtained. These results show that our analytical theory yields a good approximation even beyond the parameter regime for which it is derived.

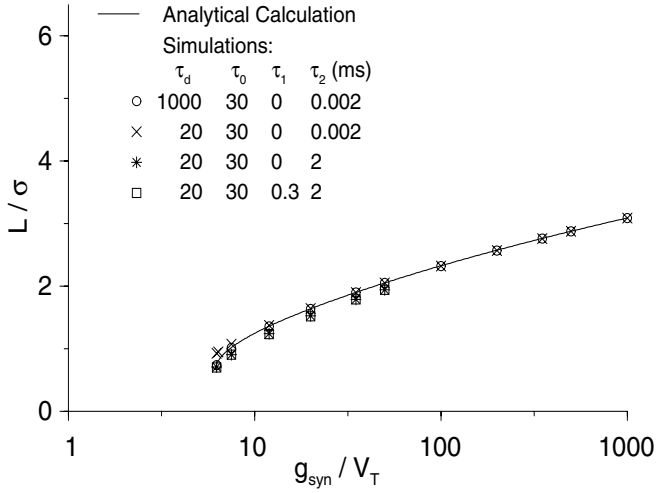

Figure 7. The normalized length of the lurching period L/σ as a function of $g_{\rm syn}/V_T$ for the Gaussian footprint shape. The analytical solution is given by equation (42). Simulations were carried out with $N = 200\,000$ and $\rho = 500$. The analytical solution for the case of $\tau_1 = 0$, $\tau_2 \ll \tau_0 \ll \tau_d$ is represented by the solid line. Simulation results with a corresponding parameter set: $\tau_d = 1000$ ms, $\tau_0 = 30$ ms, $\tau_1 = 0$, $\tau_2 = 0.002$ ms, denoted by ○, fit the analytical solutions almost exactly. The symbol × denotes simulations with $\tau_d = 20$ ms, $\tau_0 = 30$ ms, $\tau_1 = 0$, $\tau_2 = 0.002$ ms; the symbol ⋆ denotes simulations with $\tau_d = 20$ ms, $\tau_0 = 30$ ms, $\tau_1 = 0$, $\tau_2 = 2$ ms; and the symbol □ denotes simulations with $\tau_d = 20$ ms, $\tau_0 = 30$ ms, $\tau_1 = 0.3$, $\tau_2 = 2$ ms.

3.3.3. Footprint shapes with finite support. Suppose that the footprint shape has a finite support: $w(x) = 0$ for $x > \sigma$. The RHS of equation (39) is zero for $L \geqslant \sigma$, and therefore $L < \sigma$ for every $g_{\rm syn}$. For the square footprint shape, substituting equation (7) in equation (39) yields

$$\frac{V_T}{g_{\rm syn}} = \begin{cases} \dfrac{L}{2\sigma} & 0 \leqslant L \leqslant \sigma/2 \\ \dfrac{1}{2}\left(1 - \dfrac{L}{\sigma}\right) & \sigma/2 < L \leqslant \sigma. \end{cases} \tag{44}$$

The maximum of the RHS of equation (44) is obtained for $L = \sigma/2$ for $V_T/g_{\rm syn} = 1/4$. Therefore, a threshold for the propagation of the lurching pulse is $g_{\rm syn} = 4V_T$, for which $L = \sigma/2$. For larger $g_{\rm syn}$-values, L is given by

$$L = \sigma\left(1 - \frac{2V_T}{g_{\rm syn}}\right). \tag{45}$$

3.4. The nature of lurching pulses

The boundary condition that $\phi(x) \to \infty$ as $x \to L$ is necessary for obtaining equation (39). The meaning of this condition is that for the spatially continuous dynamical system defined by equations (2), (3), the function $T(x)$ for the lurching pulse is continuous in x (although not smooth). The firing time of neurons at the edge of each lurching spatial period increases rapidly as x approaches the edge. When this time reaches the value $T_{\rm per}$ (of order τ_d), a new lurching period starts. As seen in figure 6, $\phi(x)$ increases considerably only in a narrow spatial

regime near $x = L$. The discontinuous lurching period seen in figure 1 is a result of the discrete nature of our numerical simulation. On a discrete lattice, the value of ϕ (and that of f) must be finite. Our numerical simulations show that for $\tau_d \gg \tau_{dc}$, the value of f for the last neuron in a spatial lurching period is smaller than $T_{\rm per}$, creating an effect which looks like a discontinuity.

3.5. Finite axonal velocity

The effects of finite axonal velocity c on the velocity v are studied by substituting the condition for a continuous pulse into equation (10) to obtain

$$\int_0^\infty \mathrm{d}x'\, w\left(x' + \frac{\tau_d}{1/v - 1/c}\right) G\left[x'\left(\frac{1}{v} - \frac{1}{c}\right)\right] = \frac{V_T}{g_{\rm syn}}. \tag{46}$$

This equation is similar to equation (15) except that the velocity v in equation (15) is replaced by the term v_∞, where

$$\frac{1}{v_\infty} = \frac{1}{v} - \frac{1}{c}. \tag{47}$$

The velocity v_∞ is the pulse velocity in the limit $c \to \infty$. This means that the effects of axonal conduction velocity on the velocity of the continuous waves can be deduced from first studying the properties of a model with $c \to \infty$ and calculating the velocity v_∞, and then substituting for the value v_∞ with the value $1/v - 1/c$ (figure 8). Similarly, the stability of the continuous pulse is determined by an equation similar to equation (17), except that the variable v in that equation is replaced by v_∞. As a result, the value of τ_{dc} for a specific value of $g_{\rm syn}$ does not depend on c.

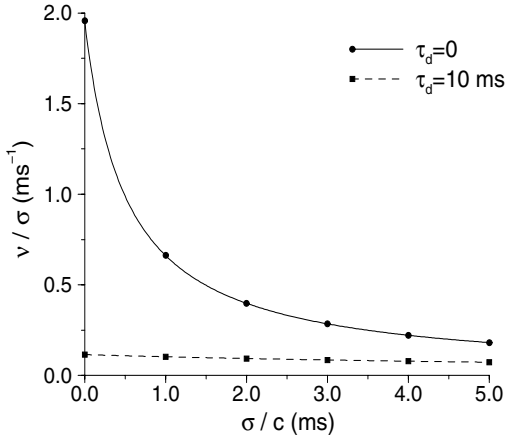

Figure 8. Effects of finite axonal conductance velocity c. The normalized velocity of the continuous pulse v/σ is plotted as a function of σ/c. Analytical results (equation (47)) are denoted by a continuous line for $\tau_d = 0$ and by a dashed line for $\tau_d = 10$ ms. Simulation results are denoted by solid circles ($\tau_d = 0$) and by solid squares ($\tau_d = 10$ ms). Parameters: $\tau_0 = 30$ ms, $\tau_2 = 2$ ms, $g_{\rm syn}/V_T = 10$, $N = 5000$, $\rho = 50$.

3.6. Thalamic model

Concerning the square footprint shape, three main new results have emerged from studying the present integrate-and-fire model in which each neuron can fire only one spike:

(I) The continuous pulse is stable over a broader parameter range in comparison to that for the exponential footprint shape.
(II) A bistable parameter regime, in which both continuous and lurching pulses can propagate, is observed.
(III) There are 'tongues' in the phase diagram.

These results can be tested in a biophysical, conductance-based model of thalamic networks. Here, we choose the RE–TC model of Golomb *et al* (1996). The TC-to-RE AMPA conductance g_{AMPA} corresponds to g_{syn} in the reduced model. The effective delay depends on several parameters of the model, In particular, it depends on the strength of the RE-to-TC $\mathrm{GABA_B}$ conductance.

Computing the phase diagram of the full biophysical model in practice is a difficult and time consuming. Moreover, in addition to the states of the integrate-and-fire model, there are other, more disordered states (see below). We have run several simulations to examine whether the three predictions of the integrate-and-fire model listed below are confirmed also in the conductance-based model.

(I) *Continuous pulses.* For the square footprint shape, the wave can lurch at low g_{AMPA} and propagate continuously at the front at larger g_{AMPA}, as shown in the rastergrams in figure 9. After the front has propagated, oscillations remain, because neurons in the full model can fire many (calcium) spikes. At very large g_{AMPA}, the front may be aperiodic (not shown), probably because of the effects of secondary (and more) spikes. With all the simulations with exponential footprint shape, we have not found continuous pulses. This is consistent with our theory for the integrate-and-fire model, in which, for exponential shape, continuous pulses are observed only for relatively small τ_d.
(II) *Bistability.* Finding the full extent of the continuous and lurching regimes in the full model is difficult. To show that there is bistability, however, it is enough to find one parameter set for which different types of propagation occur for different initial conditions. The network dynamics is demonstrated in the rastergrams in figure 10. When the wave is initiated by a 'shock' in the RE cells, a lurching wave emerges. When the wave is initiated by a 'shock' in the TC cells, a continuous wave emerges. With these particular two initial conditions, we have found bistability in a restricted parameter regime.
(III) *Tongues.* In our simulations of the full RE–TC model with square pulses, we have not successfully found 'tongues' as in the integrate-and-fire model. As g_{AMPA} increases, we see a transition from a lurching wave to a continuous wave (with some bistable regime), and then a transition to a disordered front. A possible factor that may smear the tongues is the effect of subsequent spikes (following the first one) on the propagation of the discharge front.

4. Discussion

In this work, we have studied the propagation of pulses in one-dimensional networks of integrate-and-fire neurons. The simplification that each neuron can fire only one spike enables us to study the model analytically. The main results of this work are:

(1) Continuous pulses can propagate along one-dimensional neuronal networks with small constant delay τ_d, and lurching pulses can propagate with large τ_d.
(2) The propagation velocity is hardly affected by the pulse type.
(3) The propagation velocity of both continuous and lurching pulses at large g_{syn} depends on the tail of the footprint shape $w(x)$. The velocities depend logarithmically on g_{syn} for an

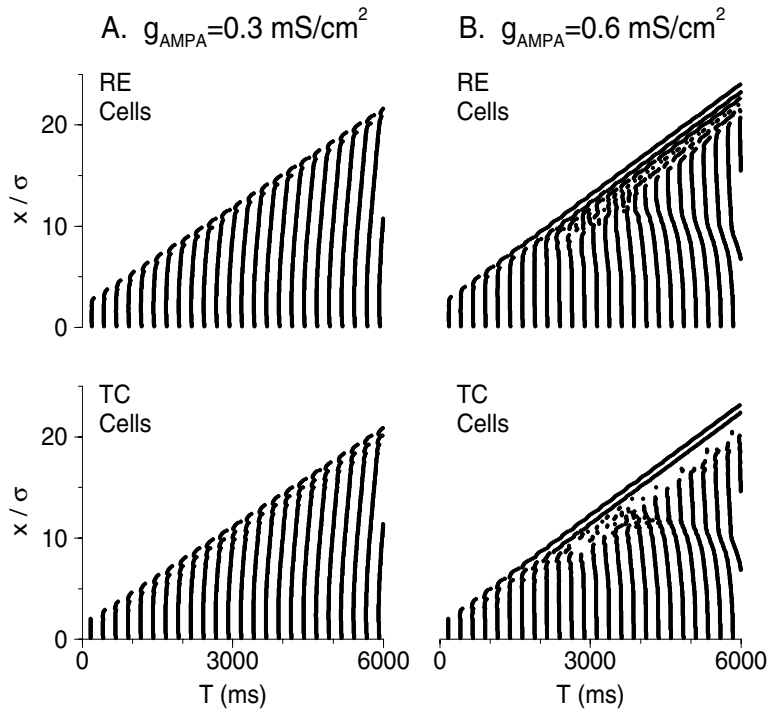

Figure 9. Rastergrams of the RE–TC model (Golomb *et al* 1996): firing times of RE cells are shown in the upper panels, and firing times of TC cells are shown in the lower panels. Each RE cell projects to one TC cell; each TC cell projects to RE cells with a square footprint shape and density of cells $\rho = 8$ (eight cells within a footprint length σ). Activity is initiated by a 'shock' in the RE cells. (A) For small AMPA conductance ($g_{\mathrm{AMPA}} = 0.3$ mS cm^{-2}, left), the wave lurches at the front, as the front is not continuous. (B) For larger AMPA conductance ($g_{\mathrm{AMPA}} = 0.6$ mS cm^{-2}, right), the wavefront is continuous, with an oscillatory wake.

exponential footprint shape; they increase as $\sqrt{\ln(g_{\mathrm{syn}})}$ for a Gaussian footprint shape, and are bounded by σ/τ_d for any footprint shape with finite support, including the square footprint shape.

(4) The footprint shape strongly affects the types of pulse that are obtained with intermediate τ_d and g_{syn}. In particular, bistability can occur with Gaussian or square shape (or with an off-centre shape (Rinzel *et al* 1998)) but not with exponential shape.

(5) Bistability and tongues can be obtained even with footprint shapes that do not have finite support.

(6) Finite, small values of the rise time τ_1 do not have a significant effect on the velocity and the stability of either continuous or lurching pulses, as long as τ_d is not too small.

(7) The axonal conductance velocity c reduces the velocity of continuous pulses according to the rule $1/v = 1/v_\infty + 1/c$, and does not affect the critical delay τ_{dc}.

4.1. Contribution of analytical treatment and effects of approximations

In the present work, we are interested in the process of recruitment of neurons into the activity. It does not deal with the period of firing and its termination. The simplification that each neuron is allowed to fire only one spike is justified for cortical tissues, in particular with prominent

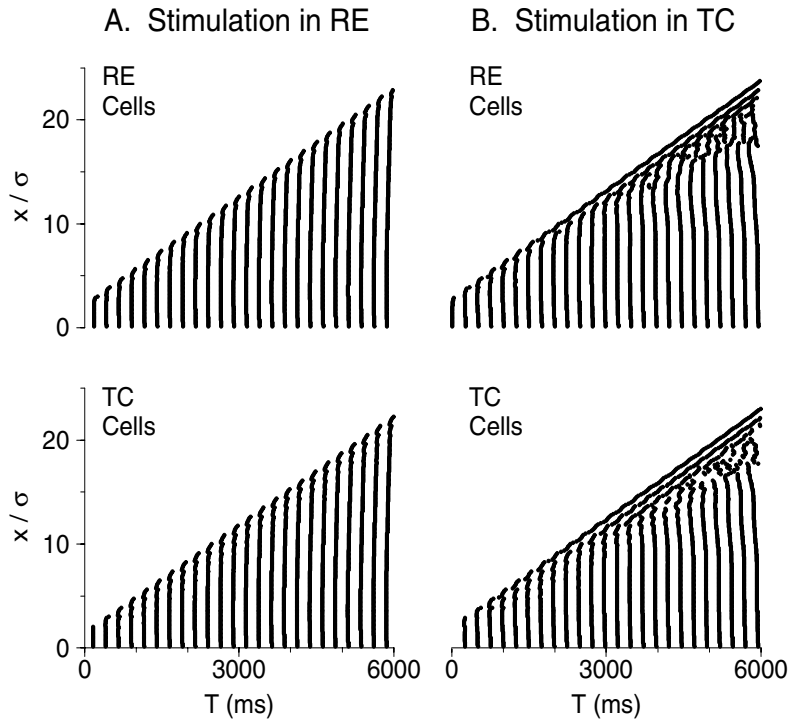

Figure 10. Rastergrams of the RE–TC model as in the previous figure, with the same architecture and parameters as in figure 9, and AMPA conductance $g_{\mathrm{AMPA}} = 0.46$ mS cm^{-2}. When activity is initiated by a 'shock' in the RE cells (A), the wavefront lurches. When the shock is given to the TC cells (B), the wavefront is continuous.

synaptic depression, because the velocity is determined primarily by the response to the first pre-synaptic spike. It is justified for the thalamic network because of the large effective delay, except for the parameter regimes discussed below.

The one-dimensional integrate-and-fire model with one spike only is simple enough to be amenable to analytical treatment. This treatment enables us to understand the general properties of continuous and lurching pulses. Specifically, it explains the mathematical reason for the existence of a minimal velocity below which the continuous pulse cannot propagate: there is the saddle-node bifurcation in which the upper branch of pulses coalesces with the lower, unstable branch, and they both disappear. The analysis shows that the lurching pulse emerges as a result of the destabilization of the continuous pulse via a Hopf bifurcation when the delay is larger than a critical value τ_{dc}. It enables us to calculate the pulse velocity as a function of the network parameters, and yields a simple formula for estimating the effects of finite axonal velocities. Our work shows that the functional dependencies of the velocities of the continuous and the lurching pulses on g_{syn} are similar for large g_{syn}, and are determined by the tail of the synaptic footprint shape. If the Hopf bifurcation is supercritical, the deviation of the velocity of the lurching pulse from the velocity of the unstable continuous pulse grows linearly with $\tau_d - \tau_{dc}$ for $\tau_d \geqslant \tau_{dc}$.

The generality of the results obtained by analysing our simple model can be assessed by comparing them with results obtained from more biophysical, conductance-based models. For large τ_d, the simple model is compared with a model of thalamic slices (Golomb *et al* 1996).

The dependences of the velocity of lurching pulses in the two models seem consistent; in both cases the velocity increases logarithmically with g_{syn} for an exponential footprint shape and is bounded for a square footprint shape. In the conductance-based model with a square footprint shape, there is a transition from a lurching pulse to a continuous pulse as the AMPA conductance strength g_{AMPA} increases, with possible bistability. This is analogous to the similar transition obtained in the integrate-and-fire model as g_{syn} increases. For small τ_d, the simple model is compared with a model of disinhibited cortical slices (Golomb and Amitai 1997). The dependences of the velocity on g_{syn} in the two models are similar. In particular, both systems have a minimal velocity below which the pulse cannot propagate.

Investigating the dynamics of sparse neuronal networks (Golomb and Hansel 2000, Golomb *et al* 2000) revealed that when synchrony of spikes is concerned, integrate-and-fire models exhibit qualitatively different behaviour to conductance-based models. Here we show that when propagation of discharge fronts is concerned, integrate-and-fire models can sufficiently describe important aspects of the network dynamics. The difference between the two cases probably stems from the different roles the details of the spike-generating mechanism play in the two dynamical phenomena. Synchronization of spikes depends strongly on these details. In contrast, the propagation of a discharge front is mainly determined by the level and rate of depolarization a cell receives before it reaches the threshold and fires; details of the spike-generating mechanism play only a minor role. Intrinsic ionic properties, however, strongly affect the spatio-temporal properties of the discharge beyond the front, as well as the mechanisms for discharge termination.

The approximation that each neuron can fire only one spike has several consequences for the discharge activity. With respect to thalamic networks, the effect of subsequent spikes enables the propagation of lurching discharge with very low velocities (Golomb *et al* 1996), whereas there is a minimal finite velocity for lurching pulses with only one spike. This effect of subsequent spikes probably contributes to the smearing of the bistable tongues, that are seen, for square or Gaussian footprint shapes, with the integrate-and-fire model but not with the conductance-based model. In order to describe the behaviour of the discharge after the front has passed and the process that leads to its termination, one has to take into account all of the spikes that a neuron can fire, in addition to the intrinsic and synaptic ionic processes that cause the spike termination (Bal and McCormick 1996, Destexhe *et al* 1996, Golomb and Amitai 1997).

4.2. Comparison with previous work

The instability of continuous pulses with large τ_d has been shown independently by Bressloff (2000). Here we find that lurching pulses are obtained at these values of τ_d, and sometimes even coexist with the continuous pulses, and study the dependence of the properties of continuous and lurching pulses on the footprint shape. Traub and colleagues (Miles *et al* 1988, Traub *et al* 1993) have studied numerically the velocity reduction due to finite c. Here, we find a simple analytical formula that relates the velocity with finite c to the velocity in the limit $c \to \infty$. A heuristic argument showing that the velocity of the lurching pulse increases logarithmically with g_{syn} at large g_{syn} was presented in the work of Golomb *et al* (1996) (but see also Chen *et al* 1998). Here we derive, using a perturbation calculation (asymptotic expansion), the exact relationship between the velocity and g_{syn} in the limit $\tau_2 \ll \tau_0 \ll \tau_d$ for any footprint shape $w(x)$. For the exponential and the Gaussian cases, we show that this result is still a good approximation well beyond this limited parameter regime.

In this work, the thalamic network model is reduced to a network of reticular thalamic neurons coupled with effective excitation with delay. Rinzel *et al* (1998) have reduced the same

network to a system of thalamocortical cells coupled by effective inhibition. The two pictures are complementary. Our reduction is exact in the limit $\sigma_{IE} \ll \sigma_{EI}$, where σ_{IE} and σ_{EI} denote the inhibitory-to-excitatory and the excitatory-to-inhibitory footprint length respectively, whereas the reduction of Rinzel *et al* (1998) is exact in the limit $\sigma_{IE} \gg \sigma_{EI}$. Experimental results and computational models indicate that the sum of these two lengths is small, of order 100 μm (Destexhe *et al* 1996, Golomb *et al* 1996), but there is as yet no direct measure of each length separately. Rinzel *et al* (1998) showed that propagation can proceed smoothly with an off-centre footprint shape in a parameter regime in which lurching occurs with an on-centre footprint shape; in some parameter regime, the wave can lurch in one direction and propagate smoothly in the other direction. Here we show more generally that the parameter regime in which lurching or smooth propagation occurs depends on the footprint shape. The different types of propagation in the two directions are an indication of bistability in that system, as we find with a square footprint shape.

In Terman *et al* (2000) a conductance-based model related to that in Rinzel *et al* (1998) is analysed using singular perturbation methods. The existence of smooth and lurching waves is established by rewriting the integro-differential equations as a boundary-value problem. Since the footprint used in this work is the 'square' footprint, the resulting equation is defined on a finite spatial interval and can be numerically solved using AUTO (Doedel 1981). Formulae for the velocity of the waves are given as functions of the synaptic strength and the time constants of the synapses. The velocity does not depend so strongly on the synaptic strength as in the present model, but this is probably due to the limited range of strengths studied in Terman *et al* (2000). The strongest effect on the wave velocity comes from a parameter which governs the effective delay (related to our parameter τ_d). Since there is no *a priori* assumption that a single spike is emitted, a variety of other types of waves are described in Terman *et al* (2000), and the behaviour of the medium after the wave has passed is also described.

Pulse propagation in networks of integrate-and-fire-type neurons has also been studied by Fohlmeister *et al* (1995), Horn and Opher (1997), and Kistler *et al* (1998). The application of the Volterra formulation (equation (10)) of the integrate-and-fire model for pulse propagation in locally coupled networks was introduced also by Kistler *et al* (1998). This formalism resembles the spike response model of Gerstner and colleagues (Gerstner 1995, Gerstner *et al* 1996, Kistler *et al* 1997).

4.3. Consequences for experimental preparations

Our model constitutes a framework for comparing and explaining the velocities and types of pulses and waves in various tissues, whose dynamics can be reduced to that of equation (2), (3). The main reason that thalamic spindle-like waves propagate much more slowly than paroxysmal discharges in the neocortex, hippocampus, and piriform cortex is that the effective delay in the thalamic network is much longer ($\sim$100 ms in comparison to $\sim$2 ms in the cortex). When inhibition is mediated by $GABA_B$ inhibition only, the time needed for a TC neuron to rebound from hyperpolarization is larger in comparison to the case when $GABA_A$ inhibition is intact; the number of Na^+ action potentials within a burst is more prolonged (Bal *et al* 1995a, b), which may result in a stronger effective g_{syn}. The combined effect is that the velocity is reduced with $GABA_A$ blockade (Destexhe *et al* 1996, Golomb *et al* 1996, Kim *et al* 1995).

Paroxysmal discharges propagate in slices of neocortical layer IV with a velocity which is about an order of magnitude smaller than the propagation velocity in cortical slices (Fleidervish *et al* 1998). The slow velocity is partly explained by the fact that these discharges are mediated by slow NMDA receptors (larger τ_1 and τ_2; see equations (4), (18), (25)) but assuming that the footprint length in layer IV is small in comparison to that in layer V, which mediates mostly

the propagation in coronal slices (Telfeian and Connors 1998), is also necessary to explain the slow velocity. Measurements of the critical velocity v_c, together with our theoretical model, should be carried out in order to estimate the footprint length in layer IV networks.

Acknowledgments

We are grateful to C van Vreeswijk, D Hansel, J Rinzel, M J Gutnick, and E Barkai for helpful discussions. This research was supported by Grant No 9800015 from the United States–Israel Binational Science Foundation (BSF), Jerusalem, Israel, to DG and GBE; GBE is funded by NSF and NIMH.

Appendix A. Stability of the lower branch

Here, following the ideas of Bressloff (2000), we prove that the branch of solutions with slow velocity are unstable. Recall that the velocity satisfies the implicit equation (equation (15))

$$\frac{V_T}{g_{\rm syn}} = \int_0^\infty w(x' + v\tau_d)G(x'/v)\,{\rm d}x'. \tag{A.1}$$

We differentiate this implicitly to get ${\rm d}v/{\rm d}g_{\rm syn}$:

$$-\frac{V_T}{g_{\rm syn}^2}\frac{{\rm d}g_{\rm syn}}{{\rm d}v} = \int_0^\infty {\rm d}x' \left[\tau_d w'(x' + v\tau_d)G(x'/v) - \frac{x'}{v^2}w(x' + v\tau_d)G'(x'/v)\right]. \tag{A.2}$$

Using the fact that $G(0) = 0$, an integration by parts of the first term in the integral yields

$$-\frac{V_T}{g_{\rm syn}^2}\frac{{\rm d}g_{\rm syn}}{{\rm d}v} = \int_0^\infty {\rm d}x' \left[-\frac{\tau_d}{v}w(x' + v\tau_d)G'(x'/v) - \frac{x'}{v^2}w(x' + v\tau_d)G'(x'/v)\right]. \tag{A.3}$$

Thus, we have the following result:

$$\frac{V_T}{g_{\rm syn}^2}\frac{{\rm d}g_{\rm syn}}{{\rm d}v} = \frac{1}{v^2}\int_0^\infty {\rm d}x'\ (x' + v\tau_d)w(x' + v\tau_d)G'(x'/v). \tag{A.4}$$

This means that on the slow branch (where ${\rm d}v/{\rm d}g_{\rm syn} < 0$ and therefore ${\rm d}g_{\rm syn}/{\rm d}v < 0$), the integral is negative.

The stability equation (equation (17)) is

$$0 = H(\lambda) \equiv \int_0^\infty {\rm d}x'\ w(x' + \tau_d v)G'\left(\frac{x'}{v}\right)\left[1 - {\rm e}^{-\lambda(x' + \tau_d v)}\right]. \tag{A.5}$$

Clearly $H(0) = 0$ (corresponding to translation invariance). Differentiating this with respect to λ and evaluating at $\lambda = 0$ yields

$$\frac{{\rm d}H}{{\rm d}\lambda}(0) = \int_0^\infty {\rm d}x'\ w(x' + \tau_d v)G'\left(\frac{x'}{v}\right)(x' + v\tau_d) \tag{A.6}$$

and from (A.4), we see that

$$\frac{{\rm d}H}{{\rm d}\lambda}(0) = \frac{v^2 V_T}{g_{\rm syn}^2}\frac{{\rm d}g_{\rm syn}}{{\rm d}v}. \tag{A.7}$$

Thus, on the slow branch, ${\rm d}H/{\rm d}\lambda(0) < 0$. Thus, for λ real and close to zero, $H(\lambda) < 0$. Now, clearly,

$$H(\infty) = \int_0^\infty {\rm d}x'\ w(x' + v\tau_d)G'\left(\frac{x'}{v}\right). \tag{A.8}$$

Suppose that $w(x)$ is differentiable. Then we can integrate the above by parts, obtaining

$$H(\infty) = -\nu \int_0^\infty \mathrm{d}x'\; w'(x' + \nu\tau_d) G\left(\frac{x'}{\nu}\right). \tag{A.9}$$

If $w(x)$ is monotonically decreasing and $G(t) \geqslant 0$, then we see that $H(\infty) > 0$. Since $H(\lambda) < 0$ for λ small and $H(\lambda) > 0$ for sufficiently large λ, we conclude that there must be at least one positive real root λ_0 of $H(\lambda)$ and therefore the slow (lower) branch is unstable.

References

Bal T and McCormick D A 1996 What stops synchronized thalamocortical oscillations? *Neuron* **17** 297–308

Bal T, von Krosigk M and McCormick D A 1995a Synaptic and membrane mechanisms underlying synchronized oscillations in the ferret lateral geniculate nucleus *in vitro*, *J. Physiol. Lond.* **483** 641–63

Bal T, von Krosigk M and McCormick D A 1995b Role of ferret perigeniculate nucleus in the generation of synchronized oscillations *in vitro*, *J. Physiol. Lond.* **483** 665–85

Bressloff P C 1999 Synaptically generated wave propagation in excitable neural media *Phys. Rev. Lett.* **82** 2979–82

Bressloff P C 2000 Traveling waves and pulses in a one-dimensional network of excitable integrate-and-fire neurons *J. Math. Biol.* **40** 169–98

Chen Z, Ermentrout B and Wang X-J 1998 Wave propagation mediated by GABAB synapse and rebound excitation in an inhibitory network: a reduced model approach *J. Comput. Neurosci.* **5** 53–69

Chervin R D, Pierce P A and Connors B W 1988 Periodicity and directionality in the propagation of epileptiform discharges across neocortex *J. Neurophysiol.* **60** 1695–713

Connors B W 1984 Initiation of synchronized neuronal bursting in neocortex *Nature* **310** 685–7

Demir R, Haberly L B and Jackson M B 1998 Voltage imaging of epileptiform activity in slices from rat piriform cortex: onset and propagation *J. Neurophysiol.* **80** 2727–42

Destexhe A, Bal T, McCormick D A and Sejnowski T J 1996 Ionic mechanisms underlying synchronized oscillations and propagating waves in a model of ferret thalamic slices *J. Neurophysiol.* **76** 2049–70

Doedel E 1981 AUTO: a program for the automatic bifurcation analysis of autonomous systems. *Cong. Num.* **30** 265–84

Ermentrout G B 1998 The analysis of synaptically generated traveling waves *J. Comput. Neurosci.* **5** 191–208

Fohlmeister C, Gerstner W, Ritz R and van Hemmen J L 1995 Spontaneous excitations in the visual cortex: stripes, spirals, rings, and collective bursts *Neural Comput.* **7** 905–14

Fleidervish I A, Binshtok A M and Gutnick M J 1998 Functionally distinct NMDA receptors mediate horizontal connectivity within layer 4 of mouse barrel cortex *Neuron* **21** 1055–65

Gerstner W 1995 Time structure of the activity in neural network models *Phys. Rev.* E **51** 738–58

Gerstner W, van Hemmen J L and Cowan J D 1996 What matters in neuronal locking? *Neural Comput.* **8** 1653–76

Golomb D 1998 Models of neuronal transient synchrony during propagation of activity through neocortical circuitry *J. Neurophysiol.* **79** 1–12

Golomb D and Amitai Y 1997 Propagating neuronal discharges in neocortical slices: computational and experimental study *J. Neurophysiol.* **78** 1199–211

Golomb D and Ermentrout G B 1999a Continuous and lurching pulses in one-dimensional networks with delay *Soc. Neurosci. Abstr.* **25** 2196

Golomb D and Ermentrout G B 1999b Continuous and lurching traveling pulses in neuronal networks with delay and spatially-decaying connectivity. *Proc. Natl Acad. Sci. USA* **96** 13 480–5

Golomb D and Hansel D 2000 The number of synaptic inputs and the synchrony of large sparse neuronal networks *Neural Comput.* **12** 1095–139

Golomb D, Hansel D and Mato G 2000 Mechanisms of synchrony of neural activity in large networks *Handbook of Biological Physics* ed F Moss and S Gielen (Amsterdam: Elsevier Science)

Golomb D, Wang X-J and Rinzel J 1994 Synchronization properties of spindle oscillations in a thalamic reticular nucleus model *J. Neurophysiol.* **72** 1109–26

Golomb D, Wang X-J and Rinzel J 1996 Propagation of spindle waves in a thalamic slice model *J. Neurophysiol.* **75** 750–69

Gutnick M J, Connors B W and Prince D A 1982 Mechanisms of neocortical epileptogenesis *in vitro*, *J. Neurophysiol.* **48** 1321–35

Hansel D, Mato G and Meunier G 1995 Synchrony in excitatory neural networks *Neural Comput.* **7** 307–37

Hansel D, Mato G, Meunier C and Neltner L 1998 On numerical simulations of integrate-and-fire neural networks *Neural Comput.* **10** 467–83

Horn D and Opher I 1997 Solitary waves of integrate-and-fire neural fields *Neural Comput.* **9** 1677–90

Kim U, Bal T and McCormick D A 1995 Spindle waves are propagating synchronized oscillations in the ferret LGNd *in vitro*, *J. Neurophysiol.* **84** 1301–23

Kistler W M, Gerstner W and van Hemmen J L 1997 Reduction of the Hogkin–Huxley equations to a single-variable threshold model *Neural Comput.* **9** 1015–45

Kistler W M, Seitz R and van Hemmen J L 1998 Modelling collective excitation in cortical tissues *Physica* D **114** 273–95

Markram H, Lubke J, Frotscher M, Roth A and Sakmann B 1997 Physiology and anatomy of synaptic connections between thick tufted pyramidal neurones in the developing rat neocortex *J. Physiol. Lond.* **500** 409–40

Miles R, Traub R D and Wong R K 1988 Spread of synchronous firing in longitudinal slices from the CA3 region of the hippocampus *J. Neurophysiol.* **60** 1481–96

Nicolelis M A L, Baccala L A, Lin R C and Chapin J K 1995 Sensorimotor encoding by synchronous neural ensemble activity at multiple levels of the somatosensory system *Science* **268** 1353–8

Prechtl J C, Cohen L B, Mitra P P and Kleinfeld D 1997 Visual stimuli induce propagating waves of electrical activity in turtle cortex *Proc. Natl Acad. Sci. USA* **94** 7621–6

Press W H, Teukolsky S A, Vetterling W T and Flannery B P 1992 *Numerical Recipes in C* (Cambridge: Cambridge University Press)

Rinzel J and Ermentrout G B 1998 Analysis of neural excitability and oscillations *Methods in Neuronal Modeling: from Ions to Networks* 2nd edn, ed C Koch and I Segev (Cambridge, MA: MIT Press) pp 251–91

Rinzel J, Terman D, Wang X-J and Ermentrout B 1998 Propagating activity patterns in large-scale inhibitory neuronal networks *Science* **279** 1351–5

Steriade M, McCormick D A and Sejnowski T J 1993 Thalamocortical oscillations in the sleeping and aroused brain *Science* **262** 679–85

Telfeian A E and Connors B W 1998 Layer-specific pathways for horizontal propagation of epileptiform discharge in neocortex *Epilepsia* **39** 700–8

Terman D H, Ermentrout B and Yew A C 2000 Geometric singular perturbation analysis of wave propagation in thalamic networks *SIAM J. Appl. Math.* submitted

Thomson A M, Deuchars J and West D C 1993 Large, deep layer pyramid–pyramid single axon EPSPs in slices of rat motor cortex display paired pulse and frequency-dependent depression, mediated presynaptically and self-facilitation, mediated postsynaptically *J. Neurophysiol.* **70** 2345–69

Traub R D, Jefferys J G R and Miles R 1993 Analysis of the propagation of disinhibition-induced after-discharges along the guinea-pig hippocampal slice *in vitro*, *J. Physiol. Lond.* **472** 267–87

Tsau Y, Guan L and Wu J-Y 1998 Initiation of spontaneous epileptiform activity in the neocortical slice *J. Neurophysiol.* **80** 978–982

Tuckwell H C 1988 *Introduction to Theoretical Neurobiology* (Cambridge: Cambridge University Press)

von Krosigk M, Bal T and McCormick D A 1993 Cellular mechanisms of a synchronized oscillation in the thalamus *Science* **261** 361–4

Wadman W J and Gutnick M J 1993 Non-uniform propagation of epileptiform discharge in brain slices of rat neocortex *Neuroscience* **52** 255–62

Wang X-J and Rinzel J 1992 Alternating and synchronous rhythms in reciprocally inhibitory model neurons *Neural Comput.* **4** 84–97

Wolfram S 1996 *The Mathematica Book* (Cambridge: Cambridge University Press)

Wu J-Y, Tsau Y and Guan L 1999 Propagating activation during oscillations and evoked response in neocortical slices *J. Neurosci.* **19** 5005–15